Supplemental material

Schott et al., https://doi.org/10.1083/jcb.201803153

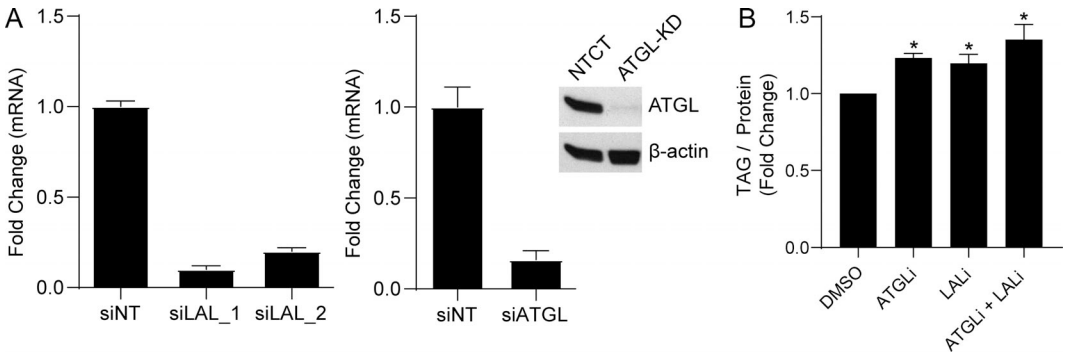

Figure S1. **Validation of siRNA knockdown and accumulation of TAG. (A)** As commercially available LAL antibodies were unsuitable for Western blot analysis, qPCR was used to validate LAL knockdown using two different siRNA pools, and ATGL knockdown by both qPCR and Western blot analysis following 72-h siRNA treatment. NTCT, nontargeting control. **(B)** To validate the effects of lipase inhibitors on triglyceride accumulation, biochemical analysis of TAG relative to total protein levels was measured in AML12 cells following 24-h treatment with DMSO, ATGLi, LALi, or ATGLi+LALi. Asterisks denote statistical significance as determined by Student's *t* test (*, P < 0.05). Graphs depict mean ± SEM from *n* = 5 experiments.

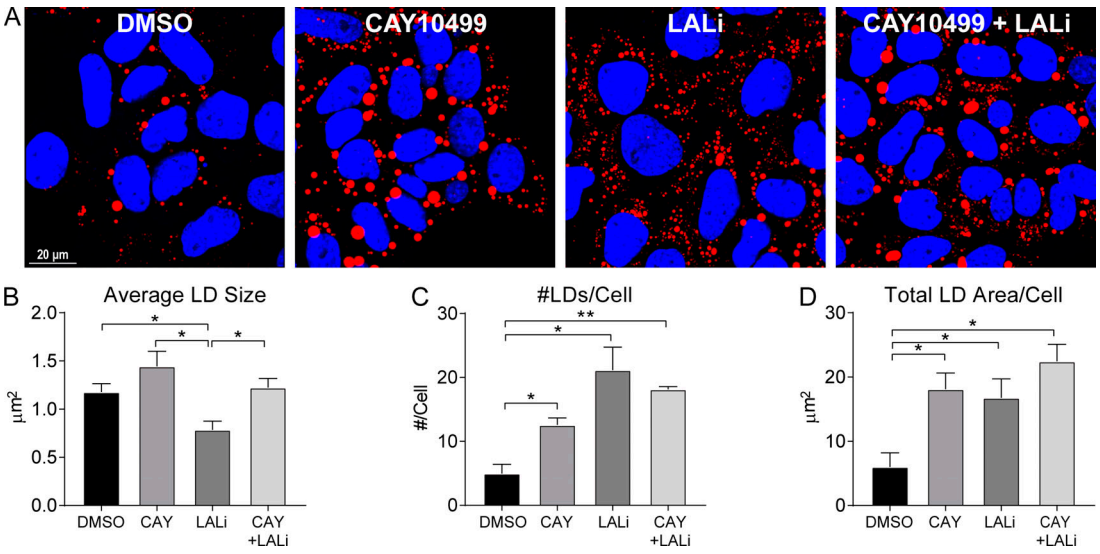

Figure S2. **The HSL/MGL inhibitor CAY10499 increases large and small LDs.** To test if inhibition of other cytosolic lipases might favor the formation of larger LDs as does ATGL inhibition, AML12 cells were loaded with OA (2 h, 150 µM) and then chased for 48 h in reduced serum medium (2% FBS, no insulin) and treated with DMSO, the HSL/MGL inhibitor CAY10499 (CAY, 12.5 µM), LALi (50 µM), or CAY+LALi. **(A)** Confocal micrographs and corresponding quantification of LDs treated with the two inhibitors revealed a 33% decrease in LD size following LALi, but this was significantly higher in cells treated with CAY+LALi or CAY alone. **(C and D)** Both LD number/cell (C) and total LD area/cell (D) were significantly increased over DMSO controls in cells treated with CAY, LALi, or CAY+LALi. Asterisks denote statistical significance as determined by one-way ANOVA and Tukey's post hoc test (*, P < 0.05; **, P < 0.01). Graphs depict mean ± SEM from *n* = 3 experiments.

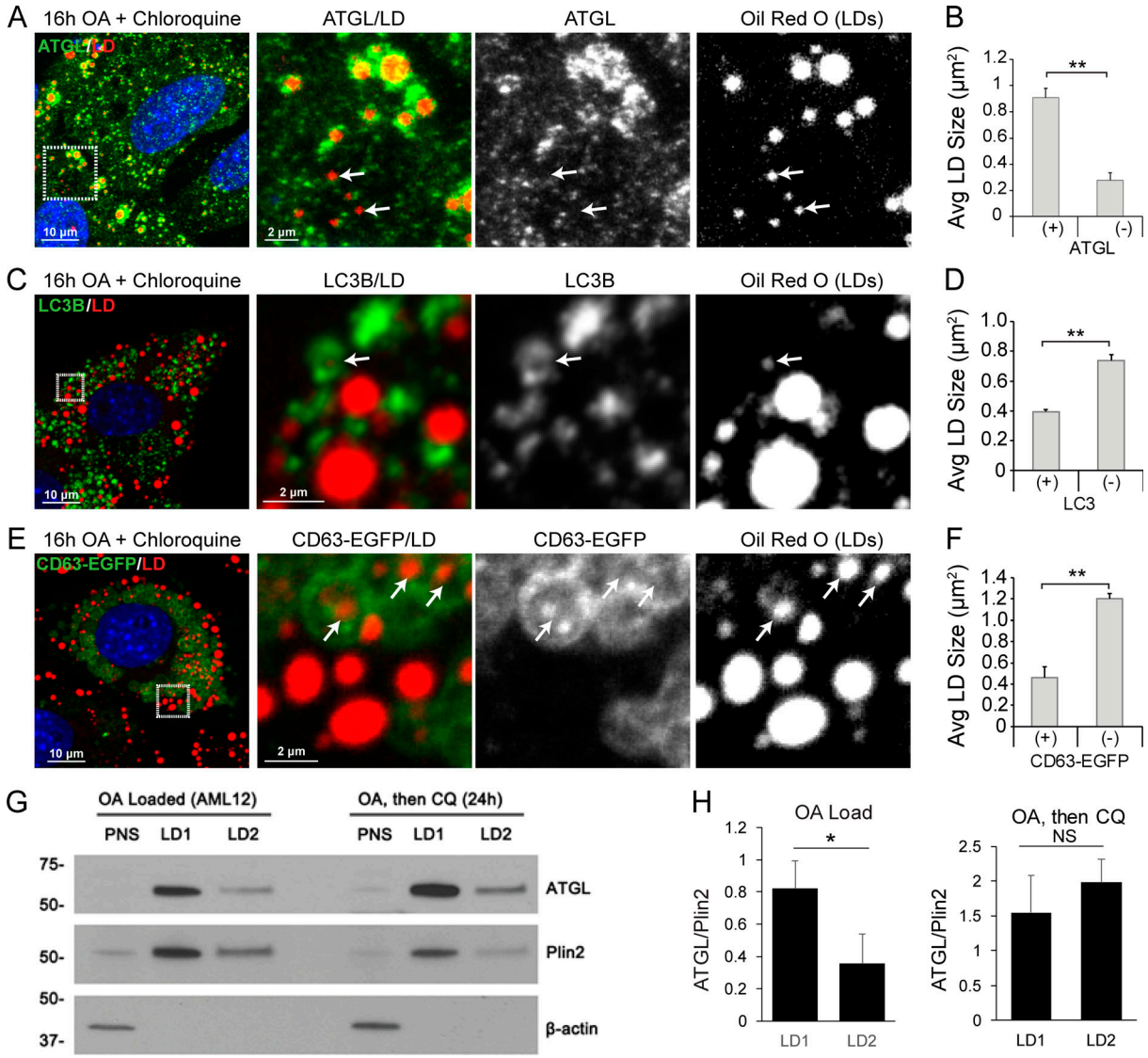

Figure S3. **LD association with lipolysis and lipophagy markers in chloroquine-treated AML12 cells. (A–F)** Representative confocal micrographs from AML12 cells loaded with OA (150 µM, 16 h) to induce LD formation, then chased for 24 h in the presence of the lysosome inhibitor chloroquine (100 µM) to "trap" LDs within a terminal lipophagic compartment. White arrows depict small LDs that are negative for ATGL in panel A, but positive for LC3 and CD63 in panels C and E, respectively. Corresponding graphs show quantification of mean size of LDs decorated in ATGL (A and B), LC3 autophagosomes (C and D), and CD63-EGFP endosomal vesicles (E and F). **(G and H)** Western blot analysis (G) and densitometry quantification (H) of LD1 and LD2 fractions from AML12 LD isolates show enrichment of ATGL in the LD1 fraction in OA-loaded cells, but 24-h treatment with chloroquine after OA load caused a redistribution of ATGL to both large and small LD fractions, suggesting that ATGL localizes more readily to small LDs in lysosome-defective cells that cannot undergo lipophagy. Asterisks denote statistical significance by Student's *t* test (*, $P < 0.05$; **, $P < 0.01$). Graphs depict mean and SEM. LD-ATGL quantification was done from a total of 120 cells, and LD-LC3 and CD63 quantification was from 30 cells each across $n = 3$ independent experiments.

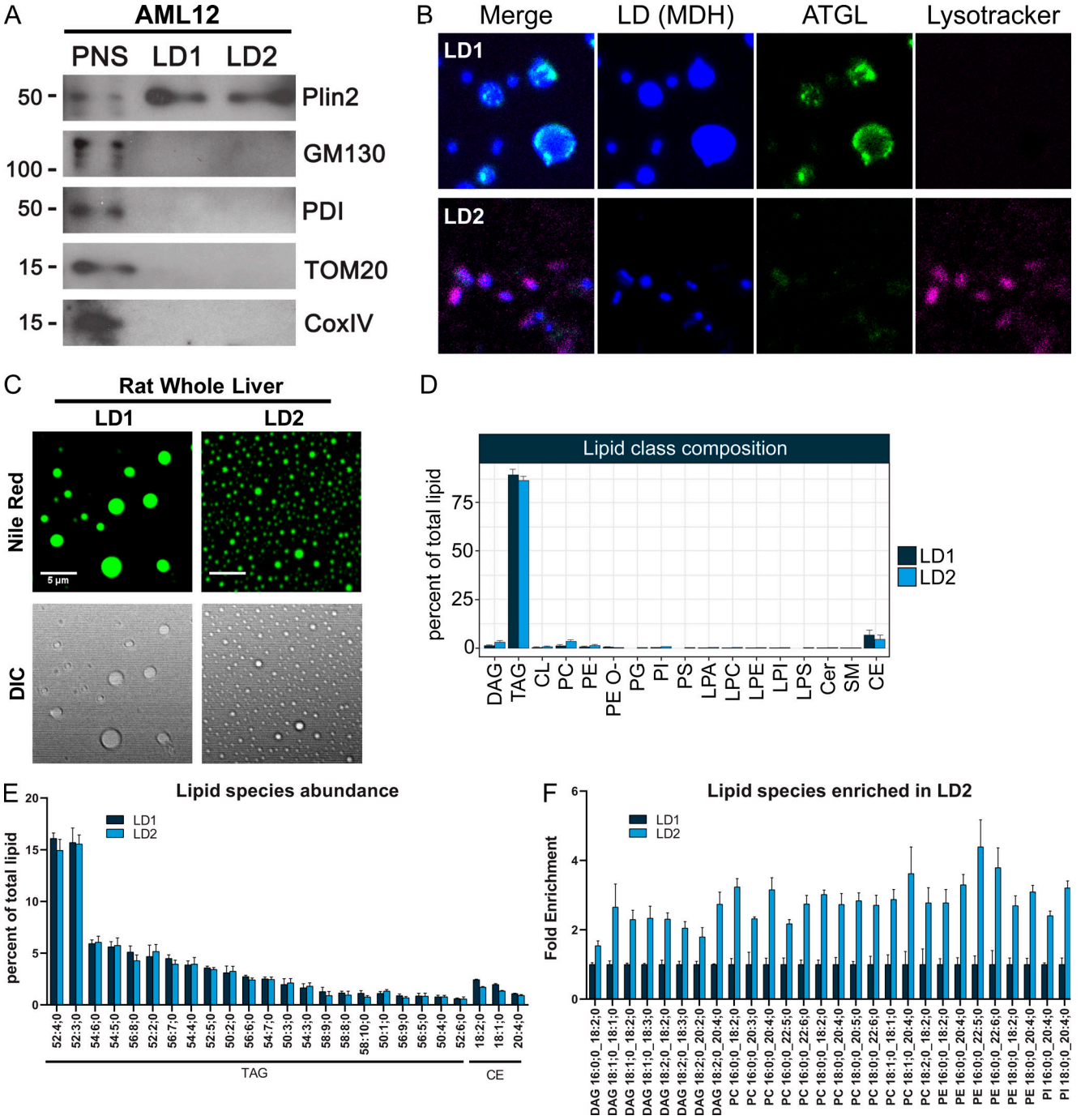

Figure S4. **Additional characterization of LD1 and LD2 fractions isolated from AML12 cells and rat whole livers. (A)** Representative Western blot from AML12 LDs shows PLIN2 enriched in LD1 and LD2 fractions containing isolated LD fractions that appear not to be enriched in Golgi (GM130), ER (protein disulfide isomerase [PDI]), or mitochondria (Tom20, CoxIV) when compared with postnuclear supernatant (PNS). **(B)** Confocal micrographs of isolated LD1 and LD2 fractions from AML12 cells plated onto poly-L-lysine–coated coverslips. Samples were immunolabeled with an ATGL antibody, stained for LDs using MDH, and stained for acidic vesicles (i.e., late endosomes, lysosomes) using LysoTracker deep red. Note that ATGL appears enriched around large LDs in the LD1 fraction, while LysoTracker-positive vesicles are virtually absent. The LD2 fraction contains numerous small LDs that appear to colocalize with LysoTracker staining, with a lack of ATGL staining. **(C)** Confocal and differential interference contrast (DIC) images of LD1 and LD2 fractions from rat whole liver stained with Nile Red. **(D)** Composition of major lipid classes within LD1 and LD2 fractions from whole rat liver shown as a percentage of overall lipid content. **(E)** Abundance of specific lipid species within LD1 and LD2 fractions shown as a percentage of total lipid content and listed in order of abundance. **(F)** Graph of individual lipids that were significantly enriched in the LD2 fraction includes several DAG, PC, PE, and PI species. Statistical significance was determined using a paired Student's *t* test ($P < 0.05$). No significant enrichment of lipid species was observed in LD1 fractions. Cer, ceramide; CL, cardiolipin; LPA, lyso-phosphatidate; LPI, lyso-PI; LPS, lyso-phosphatidylserine; PG, phosphatidylglycerol; PS, phosphatidylserine; SM, sphingomyelin. Graphs depict mean ± SD from $n = 4$ rat livers.

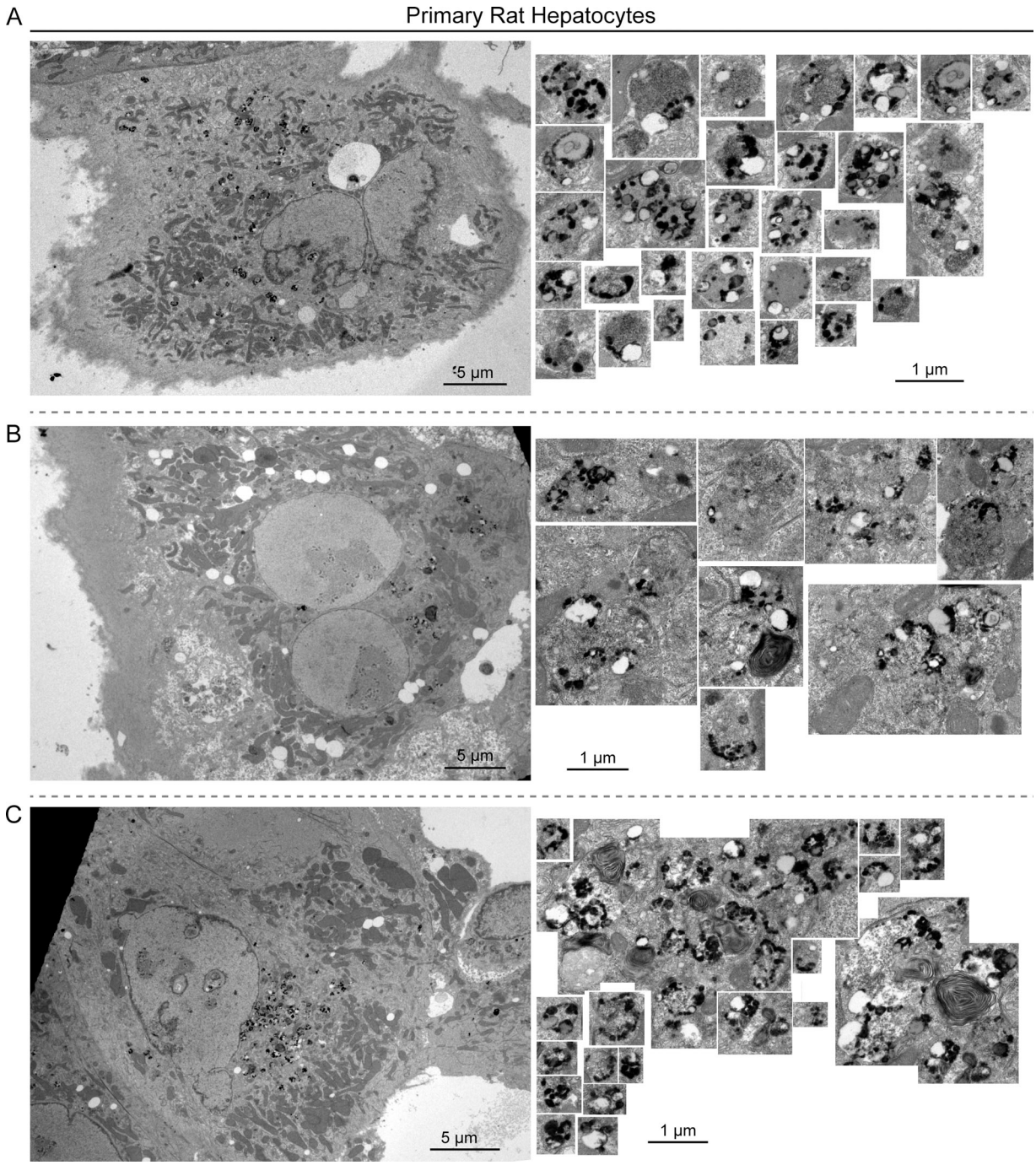

Figure S5. **Detailed ultrastructural examination of lipophagic organelles from primary hepatocytes.** Electron micrographs showing additional examples of lipophagic LDs ~250 nm in diameter in primary rat hepatocytes cultured under normal growth conditions. Many of these LDs are bound within electron-dense vesicles resembling lysosomes or late endosomes, some with examples of swirled, multilamellar membranes indicative of autolysosomes. In general, LDs were distributed toward the periphery of the vesicle lumen. Interestingly, the electron-dense staining appears to envelop the periphery of many LDs within these lipophagic vesicles. Quantification of the size of these engulfed LDs is provided in Fig. 1 C.